Review

Directing organic–inorganic hybrid molecular-assemblies of polyoxometalate crown-ether complexes with supramolecular cations

Tomoyuki Akutagawa [a,b,c,*], Daigoro Endo [b], Shin-Ichiro Noro [a,b],
Leroy Cronin [d,**], Takayoshi Nakamura [a,b,c,*]

[a] *Research Institute for Electronic Science, Hokkaido University, Sapporo 060-0812, Japan*
[b] *Graduate School of Environmental Earth Science, Hokkaido University, Sapporo 060-0810, Japan*
[c] *CREST, Japan Science and Technology Agency (JST), Kawaguchi 332-0012, Japan*
[d] *WestCHEM, Department of Chemistry, University of Glasgow, Glasgow G12 8QQ, UK*

Contents

Abstract

The design of new materials by directing the self-assembly of organic–inorganic hybrid molecular assemblies of polyoxometalate crown-ether complexes with supramolecular cations is reviewed with a particular focus on mixed-valence $[PMo_{12}O_{40}]^{4-}$ building blocks. Structurally configurable supramolecular cations of organic ammonium and crown ethers, i.e. protonated aromatic amines complexed by crown ethers are also outlined. The design principles for the one-electron reduced mixed-valence polyoxomolybdate cluster of $[PMo_{12}O_{40}]^{4-}$ are also deduced. The construction principles behind these assemblies and also the concept of using cluster-based "crowns" to complex the cations to extend the design concept further is discussed, especially in the development of inorganic crowns that could combine the properties of the electronically interesting building block along with the receptor building blocks.

* Corresponding authors at: Research Institute for Electronic Science, Hokkaido University, N12W6 kita-ku, Sapporo 060-0812, Japan. Tel.: +81 11 706 2884; fax: +81 11 706 4972.
** Corresponding author. Tel.: +44 141 330 6650; +44 141 330 4888.
E-mail addresses: takuta@es.hokudai.ac.jp (T. Akutagawa), L.Cronin@chem.gla.ac.uk (L. Cronin), tnaka@es.hokudai.ac.jp (T. Nakamura).

1. Introduction

The design and synthesis of molecular systems that exhibit pre-designed functionality on the nanoscale is one of the greatest challenges in physics, chemistry and materials science. Precise control on the nanoscale will allow the development of nanoscale devices as well as the development of materials with new, potentially exquisitely controllable properties, e.g. catalytic, magnetic and sensing [1–3]. The development of novel systems with electronic and magnetically interesting properties requires the use of building blocks where the electronic configuration and the delocalization or localization of electrons can be precisely controlled. In this context it is interesting that mixed-valence electronic and diverse spin structures have been realized using transition metal oxide cluster-based building blocks also known as polyoxometalates (POMs). Generally speaking, POM clusters are mostly anionic in nature, being based upon metal oxide building blocks with a general formula of MO_x (where M is Mo, W, V and sometimes Nb and x can be 4, 5, 6 or 7) [1–5]. The properties of metal oxide clusters are governed by the ability to generate a versatile library of linkable units and to localize and delocalize electrons in different ways to form a range of mixed valence states [2,3].

Of course, the nature of the electron delocalization within a cluster depends on the oxidation states and coordination environments of the transition metal ions through the metal–oxygen network in dimensionality and connectivity, giving different pathways for electron/state correlation within the cluster [6]. Furthermore, the delocalization of the spins or electrons within the cluster is a thermally activated hopping process of electrons or spins through the metal–oxygen network structures at finite temperature [6]. However, the metal oxide clusters have the potential to be utilized in nanoscale electronic and magnetic materials, and the use of metal oxides to produce functional nanosystems has been recently discussed [7]. Therefore, control over the cluster arrangements in the molecular-assemblies is an important point to allow the construction of nanoscale electronic and magnetic materials [4–7].

Among a large number of transition metal oxide clusters, we have been interested in structurally diverse POMs [8–11]. This is because the condensation reactions of molybdic acid derivatives under acidic conditions can form a variety of combination of corner-, edge-, and face-sharing $[MoO_x]$ units (where $x = 4$, 6, 7). Many types of POMs such as $[Mo_6O_{19}]$, $[Mo_8O_{26}]$, $[Mo_{10}O_{36}]$, $[PMo_{12}O_{40}]$, etc. and also the gigantic Mo_{132}-ball ($\equiv[Mo_{132}O_{372}(MeCO_2)_{30}(H_2O)_{72}]^{42-}$), Mo_{154}-ring ($\equiv[Mo_{154}O_{462}H_{14}(H_2O)_{70}]^{14-}$), Mo_{174}-ring ($\equiv[Mo_{176}O_{528}H_{16}(H_2O)_{80}]^{16-}$), etc., have already been characterized as two- or three-dimensional metal-oxide network structures with mixed-valence electronic structures [8–15]. The multi-stage redox properties of these POMs along with the possibility to generate mixed-valence electronic structures make them extremely attractive building block candidates for the development and design of novel electrically and magnetically active nanoscale materials. Among the mixed-valence POMs, we selected a typical one-electron reduced Keggin cluster of $[PMo_{12}O_{40}]^{4-}$ as our first building block to adjust the cluster arrangements of POMs in the crystalline state.

The compound α-$[PMo_{12}O_{40}]$ has been extensively examined from the viewpoints of catalysis [16,17], anti-viral activity [18], gas-adsorption [19], electronic [20–23], and magnetic materials [22–34]. The molecular structure of α-$[PMo_{12}O_{40}]$ can be described simply to result from the corner-sharing of 12 $[MoO_6]$ octahedrons around a central PO_4^{3-} anion, which is included at the center of the cluster [8–11]. The α-$[PMo_{12}O_{40}]^{3-}$, one-electron reduced α-$[PMo_{12}O_{40}]^{4-}$, and two-electron reduced α-$[PMo_{12}O_{40}]^{5-}$ species, with the α-Keggin structure, have been characterized in the solid state [8–11]. Although the α-$[PMo_{12}O_{40}]^{3-}$ cluster is electrically and magnetically inert due to the $(4d)^0$ electronic structure of all 12 Mo^{VI} ions, the one-electron reduced $[PMo_{12}O_{40}]^{4-}$ species with one pentavalent Mo^V ion of $(4d)^1$ electronic structure is electrically and magnetically active [20–34]. The mixed-valence electronic structure of $[PMo^V Mo^V_{11}O_{40}]^{4-}$ gives rise to the intervalence optical transition from pentavalent Mo^V to hexavalent Mo^{VI} within the cluster, and temperature dependent electron spin resonance (EPR) spectra reveals localization–delocalization spin transition [35–37]. Therefore, it can be seen that the dynamic properties of electron and spin in the mixed-valence POM system around room temperature are interesting from the point of view of constructing novel electronic and magnetic materials [38,39]. Although the mixed-valence clusters were periodically arranged within the crystal, the spin or electron has a motional freedom with quite small magnitude of activation energy on the cluster. Finally it must be emphasized that in this review we are explicitly focusing on systems that represent starting points today for the designed synthesis and assembly of new architectures. This means we have intentionally excluded many nascent and beautiful routes to the self-assembly of POMs that in the future will surely will lead to designer structures and materials. For a recent review of POMs, see Ref. [4].

2. Assembly of $[PMo_{12}O_{40}]^{3-}$-based architectures

An exceptionally large number of ionic lattices based upon the anionic $[PMo_{12}O_{40}]^{3-}$ and organic cations have been reported [4,8–15]. Although there are literally hundreds of new compounds produced in this class annually, we will focus on the notable points of crystal structures pertaining to the organic cations—$[PMo_{12}O_{40}]^{3-}$ salts and these are (i) an inclusion of large number of solvent molecules, (ii) formation of open-pore structures such as one-dimensional channel, and (iii) weak inter-cluster interactions in the solid state. Since the crystal structures of these $[PMo_{12}O_{40}]^{3-}$ salts are dominated by the electrostatic interactions between the cations and anions, the size and shape of the organic cations affect the cation–anion distance and the packing structure in the crystals [40]. Therefore, the design of the cationic units could be an highly effective strategy to control the cluster arrangements from the perspective of designing one-dimensional (1D), two-dimensional (2D), or three-dimensional (3D) network structures of $[PMo_{12}O_{40}]$-based molecular-assemblies [41–59]. Although the large and isotropic molecular structure of $[PMo_{12}O_{40}]$ sometimes caused difficulties in adopting a supramolecular building block approach [60,61], several interesting approaches have

been suggested to obtain radically different structures and these include (i) a 1D chain arrangement of lacunary $[PW_{11}O_{39}]$ clusters by introducing the alkali metal ion into the defect site of $[PW_{11}O_{39}]$ [41,42], (ii) a 2D layer arrangement of $[PMo_{12}O_{40}]^{3-}$ on the honeycomb pore structure of transition- and lanthanide-coordinated metal–organic frameworks [43–49], (iii) 2D or 3D arrangements connected by the hydrogen-bonding interaction between the organic cations and oxygen atoms of $[PMo_{12}O_{40}]^{3-}$ [43–49], and (iv) 1D or 2D arrangements by using the supramolecular cations between the metal ions and crown ethers or calixarene derivatives [19,50–59]. These approaches have been applied to form the network structures of $[PMo_{12}O_{40}]^{3-}$, while the 3D-arrangement of two-electron reduced $[PMo_{12}O_{40}]^{5-}$ clusters has been reported in the novel $(NH_4^+)[Cu_{24}I_{10}L_{10}]^{14+}[PMo_{12}O_{40}]_3^{-5}$ salt (L = 4-[3-(1H-1,2,4-triazol-1-yl)propyl]-4H-1,2,4-triazole) [62].

The combination of highly anisotropic cationic units with the relatively spherical-like $[PMo_{12}O_{40}]^{3-}$ has been reported which include supramolecular cations formed by complexation of a metal ion (M^+) within a crown ether-host [50–59]. In these salts, the alkali and/or transition metal ions are included into the cavity of crown ethers, and the size of overall cation structure can be controlled by changing the crown ether ring-size from [12]crown-4, [15]crown-5, [18]crown-6, to [24]crown-8 and/or dibenzo-substituted crown ethers. The modification of crown ethers affects the electrostatic interactions between the supramolecular cations and POM in the crystals. From the size compatibility between the supramolecular cation and POM clusters, relatively large crown ethers such as dibenzo[18]crown-6 and dibenzo[24]crown-8 have been employed for the counter cations of $[Mo_6O_{19}]^{2-}$ and $[PMo_{12}O_{40}]^{3-}$ clusters [56,58]. For example, hydrated $Cu^I(H_2O)_4$ was included into the cavity of dibenzo[24]crown-8, forming the supramolecular cation of $Cu^I(H_2O)_4$(dibenzo[24]crown-8), which yields the 1D alternate arrangements of cations and $[Mo_6O_{19}]^{2-}$ through hydrogen-bonded interactions (left-figure in Scheme 1) [58]. Within the 1D array, the inter-cluster interactions were disturbed by the existence of bulky supramolecular cations along the stack-

ing direction. The hydrated $Na^+(H_2O)_{1.5}$(dibenzo[24]crown-8) also regulated the $[Mo_6O_{19}]^{2-}$ clusters as the 1D structure [56]. Although the effective intermolecular interactions between the cation and $[Mo_6O_{19}]^{2-}$ were not observed in $Na_2^+(H_2O)_3$(dibenzo[24]crown-8)$_2[Mo_6O_{19}]$ salt, the 1D array of $[Mo_6O_{19}]^{2-}$ was obtained. By changing the size of POM from $[Mo_6O_{19}]^{2-}$ to $[PMo_{12}O_{40}]^{3-}$, the supramolecular cation of $Na^+(H_2O)_2$(dibenzo[24]crown-8) changed the cluster arrangement from a 1D chain to a 2D layer of $[PMo_{12}O_{40}]^{3-}$ (right-figure in Scheme 1) [56]. The hydrogen-bonding $[Na^+(H_2O)_2$(dibenzo[24]crown-8)$]_3$ trimer units were assembled to each other forming a 3D honeycomb porous network. The compatible diameter of $[PMo_{12}O_{40}]^{3-}$ cluster to the size of honeycomb pore organized each $[PMo_{12}O_{40}]^{3-}$ cluster to the 2D supramolecular cationic assembly. A similar approach has been reported in the honeycomb pore structures of transition metal–organic ligand frameworks [45]. The construction of 2D honeycomb pore structures, where the size of pore is necessary to fit the diameter of POM, is one useful method to array the POM clusters as the 2D layer. Although a few organic–inorganic hybrid structures with supramolecular cations between the metal ions and crown exist it is very difficult to predict the $[PMo_{12}O_{40}]$ arrangements within the crystalline assembly. The structural expansion of the supramolecular cations from the simple M^+(crown ethers) to the organic ammonium(crown ethers) has the possibility to realize diverse $[PMo_{12}O_{40}]$ arrangements in the crystals due to the structural multiplicity of these supramolecular cations. Supramolecular approaches to arrange the electron reduced $[PMo_{12}O_{40}]^{4-}$ clusters in the crystals have not yet been established. As such, work attempting to utilize an iterative design approach have focused on the one-electron reduced $[PMo_{12}O_{40}]^{4-}$ cluster-based building blocks.

3. The design of hydrogen-bonding supramolecular cations

Hydrophilic cavities of crown ethers can selectively recognize a variety of ions according to the size compatibility

M^+(dibenzo[24]crown-8)

POM
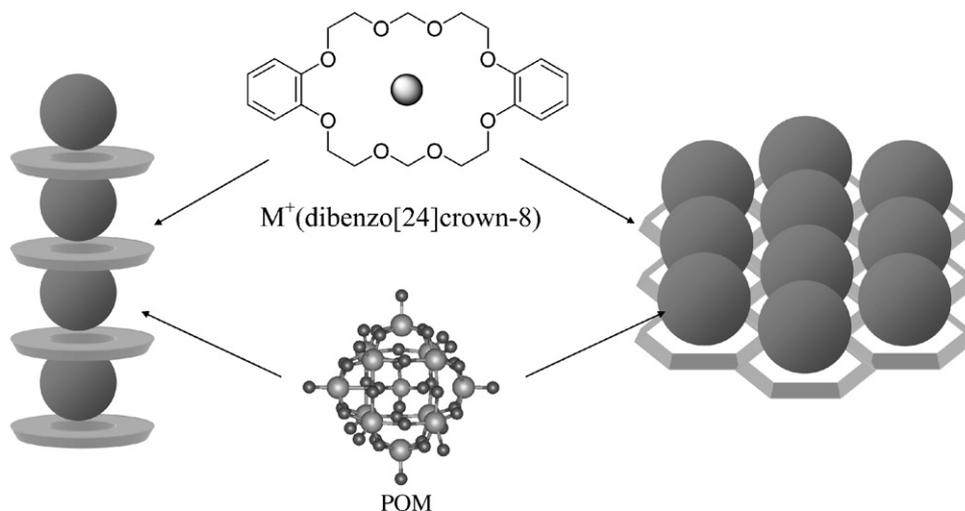
Scheme 1. Schematic representations of 1D (left) and 2D (right) arrangements of POM clusters by the aid of M^+(dibenzo[24]crown-8) cations [56,58].

between the ion and cavity since the interaction between the ion and the crown is mainly electrostatic in nature. For example, [18]crown-6 is selective for, and has high formation constants with potassium (K^+) or ammonium (NH_4^+) cations, which form the supramolecular cation structures of K^+([18]crown-6) and/or NH_4^+([18]crown-6) in solution or solid [63–66]. Since the three upper oxygen atoms of [18]crown-6 molecule are arranged at $120°$ to each other, they are pre-organized to interact with the three hydrogen atoms of the NH_4^+ ion through N–H$^+$∼O hydrogen-bonded interactions [67]. Importantly, extension from a simple NH_4^+ ion to the substituted R-NH_3^+ (R is organic substituent such as CH_3–, C_2H_5, phenyl, C_6H_5–CH_2–, etc.) gives a route to the design of supramolecular cation structures of R-NH_3^+([18]crown-6).

Thus, the introduction of supramolecular cation structures of R-NH_3^+(crown ethers) represents an effective route to adjust the supramolecular structure of the counter cations and anions in the solid state. For example, we have used these types of supramolecular cations as counter cations of the [Ni(dmit)$_2$]$^-$ anion (dmit^{2-} = 2-thioxo-1,3-dithiole-4,5-dithiolate) [68–82]. This approach allows us to modify and modulate the assembled structures of the [Ni(dmit)$_2$]$^-$ anions in the crystal, and thus to modify the magnetic properties of the [Ni(dmit)$_2$]$^-$ salts [73–80]. By using this approach, relatively large and complicated cation structures such as anilinium and p-phenylenediammonium (H2PPD^{2+}) can be introduced into the ionic crystals as counter cations. In developing this design strategy, we noticed that the mixed-valence Keggin cluster could be use as a counter cation to a variety of R-NH_3^+(crown ether) supramolecular cations. Among the range of cationic R-NH_3^+ species we choose as a structural unit to construct the supramolecular cations, for this role we selected the protonated p-phenylenediamine (PPD) derivatives as the cationic components due to the possibility of using redox active cationic motifs within the crowns. In the course of crystallization, both electron-transfer and proton-transfer processes between the electron-donor (proton-acceptor) of p-phenylenediamine (PPD) and electron-acceptor (proton-donor) of $(H^+)_3$[PMo$_{12}$O$_{40}$]$^{3-}$ yield the hydrogen-bonded supramolecular cations and the one-electron reduced mixed-valence [PMo$_{12}$O$_{40}$]$^{4-}$. The two –NH_2 sites of PPD molecule have the potential to form two kinds of cations, HPPD$^+$ and H2PPD^{2+} *via* a proton accepting process according to the reaction between PPD and $(H^+)_3$[PMo$_{12}$O$_{40}$]$^{3-}$ in solution. When the acid-dissociation constant of $(H^+)_3$[PMo$_{12}$O$_{40}$]$^{3-}$ is lower than that of PPD, complete proton-transfer from $(H^+)_3$[PMo$_{12}$O$_{40}$]$^{3-}$ to PPD occurs giving rise to the dication, H2PPD^{2+}, during the crystallization process [83,84]. Since the crown ether moiety has a much higher affinity for the cationic –NH_3^+ group than neutral –NH_2 group [63–66], both the size and shape of the supramolecular-assemblies between the HPPD$^+$ or H2PPD^{2+} and crown ethers are strongly affected by the proton-transfer state of PPD. Also, the change in cation structure will modify the arrangement of the [PMo$_{12}$O$_{40}$]$^{4-}$ cluster in the crystalline state. Therefore, we examined the combination of supramolecular cations between protonated PPDs and crown ethers by changing the size of the crown ethers from [12]crown-4, [15]crown-
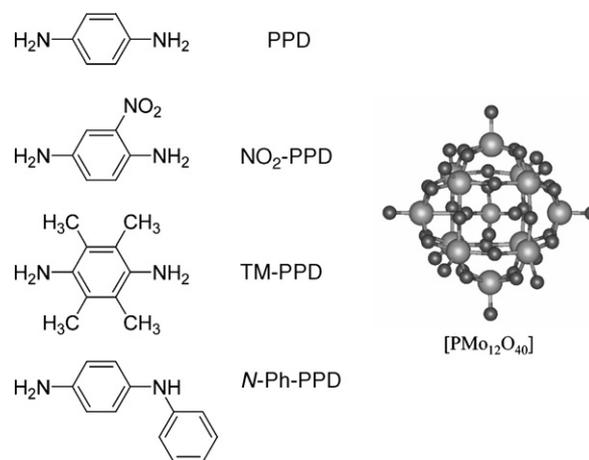
Scheme 2. Molecular structures of PPD derivatives in text and [PMo$_{12}$O$_{40}$].

5, to [18]crown-6. Furthermore, structural modification of the cationic molecules from the protonated *o*-nitro-PPD (NO$_2$-PPD), 2,3,5,6-tetramethyl-PPD (TM-PPD), to *N*-phenyl-PPD (*N*-Ph-PPD), were investigated to adjust the magnitude of intermolecular interactions for the cation and anion assemblies by using PPDs–[18]crown-6 supramolecular cation structures (Scheme 2).

4. Mixed-valence [PMo$_{12}$O$_{40}$]$^{4-}$ salts with supramolecular cations

Table 1 summarized the stoichiometries of mixed-valence [PMo$_{12}$O$_{40}$]$^{4-}$ salts (**1–6**) with the supramolecular PPD cation structures—crown ethers, in which the protonated states of the PPD derivatives in the solid state were indicated as the monoprotonated HPPD$^+$ or di-protonated H2PPD^{2+} derivatives. Since the crystal structures and magnetic properties of salts **1–3** have already been reported previously [85], we emphasize the assembled structures of the supramolecular cation, [PMo$_{12}$O$_{40}$]$^{4-}$ cluster arrangements, and the magnetic properties of salts **1–6**. From the cation structures, temperature dependent magnetic susceptibilities, and stoichiometries (elemental analyses), we deduced the protonated state of the PPD derivatives and electronic state of [PMo$_{12}$O$_{40}$] as shown in Table 1. In salts **3** and **5**, two kinds of protonated species of PPD derivatives were introduced into the crystals as a novel mixed-protonated state.

Table 1
Crystal stoichiometry of salts **1–6**

Entry	Stoichiometry[a]
1	(H$_2$PPD^{2+})$_2$([12]crown-4)$_4$[PMo$_{12}$O$_{40}$]$^{4-}$
2	(HPPD$^+$)$_4$([15]crown-5)$_4$[PMo$_{12}$O$_{40}$]$^{4-}$
3	(HPPD$^+$)$_2$(H$_2$PPD^{2+})([18]crown-6)$_4$[PMo$_{12}$O$_{40}$]$^{4-}$(CH$_3$CN)$_4$
4	(NO$_2$-HPPD$^+$)$_4$([18]crown-6)$_4$[PMo$_{12}$O$_{40}$]$^{4-}$(CH$_3$CN)$_4$
5	(TM-HPPD^{2+})$_2$(TM-PPD)$_2$([18]crown-6)$_2$[PMo$_{12}$O$_{40}$]$^{4-}$(CH$_3$CN)$_2$
6	(*N*-Ph-HPPD$^+$)$_4$([18]crown-6)$_4$[PMo$_{12}$O$_{40}$]$^{4-}$(CH$_3$CN)$_4$

[a] Determined by X-ray crystal structural and elemental analysis.

4.1. Crystal growth of mixed-valence [PMo₁₂O₄₀]⁴⁻ salts

The preparation of one-electron reduced $[PMo_{12}O_{40}]^{4-}$ salts was carried out by standard diffusion methods [86]. Typically, $(H^+)_3[PMo_{12}O_{40}]\cdot nH_2O$ (~100 mg) and PPD derivative (50 mg)–crown ethers (200 mg) were introduced into opposite sides of the H-shaped cell (50 mL) and CH_3CN (distilled prior to use) added slowly. After 10 days, single crystals were obtained as black-blocks. The slow diffusion process between $(H^+)_3[PMo_{12}O_{40}]^{3-}$ and the PPD derivatives yielded both the proton-transferred and electron-transferred states in salts **1–6**. The changes in the protonated states of the PPD derivatives modified the structures of the supramolecular cations, while the absolute magnitude of the magnetic susceptibilities of salts **1–6** were consistent with the formation of the one-electron reduced $[PMo_{12}O_{40}]^{4-}$ species (see Section 4.4). Although one-electron was transferred from the PPD derivative to $[PMo_{12}O_{40}]^{3-}$ during the formation of the extended structure, no oxidized PPD derivatives were included in the structure. However, protons were transferred from $H_3^+[PMo_{12}O_{40}]^{3-}$ to PPD, which generated mono-protonated HPPD$^+$ or di-protonated H2PPD^{2+} derivatives in the $[PMo_{12}O_{40}]^{4-}$ *via* complexation with the crown ether moieties.

Since the crown ethers are electrochemically inert, electron-transfer from the PPD electron donor to $[PMo_{12}O_{40}]^{3-}$ electron acceptor yielded the one-electron reduced $[PMo_{12}O_{40}]^{4-}$ species [87,88]. The reducibility of the $[PMo_{12}O_{40}]^{3-}$ moiety was shown by cyclic voltammetry studies in CH_3CN which indicated the reduction potential is higher than that of 7,7,8,8-tetracyano-*p*-quinodimethane (TCNQ) and similar to that of 2,5-difluoro-TCNQ, suggesting that the electron-accepting ability was high enough to cause the electron transfer from typical PPD electron donor to $[PMo_{12}O_{40}]^{3-}$ in CH_3CN [87–91]. Furthermore, the highly acidic properties of $(H^+)_3[PMo_{12}O_{40}]^{3-}$ have been reported in solution [92] and the formation of the mono-protonated HPPD$^+$ state can be expected to coexist in equilibrium with di-protonated H2PPD^{2+} state under the crystallization conditions as both the HPPD$^+$ and H2PPD^{2+} derivatives have the possibility to be included as counter cations of the $[PMo_{12}O_{40}]^{4-}$ anion species.

4.2. Electronic and spin structures of mixed-valence [PMo₁₂O₄₀]⁴⁻ salts

The electronic states of $[PMo_{12}O_{40}]^{4-}$ in salts **1–6** were evaluated by solid state UV–vis–NIR–IR spectra. Since the overall spectroscopic features of salts **1–6** were similar to each other, we show only the electronic spectrum of salt **3** in Fig. 1. The yellow-colored $(H^+)_3[PMo_{12}O_{40}]^{3-}$ has no d–d transitions (spectrum b in Fig. 1) due to fully oxidized nature of the system. The electronic absorption at 32 and 46×10^3 cm^{-1} has been assigned to metal–ligand charge transfer electronic excitation from doubly occupied oxo-orbitals to unoccupied d-orbitals of Mo^{VI} [92,93]. On the other hand, the electronic spectra of salt **3** showed broad absorption in the vis–NIR–IR energy region (spectrum a in Fig. 1). Because the octahedral coordination of six oxygen atoms
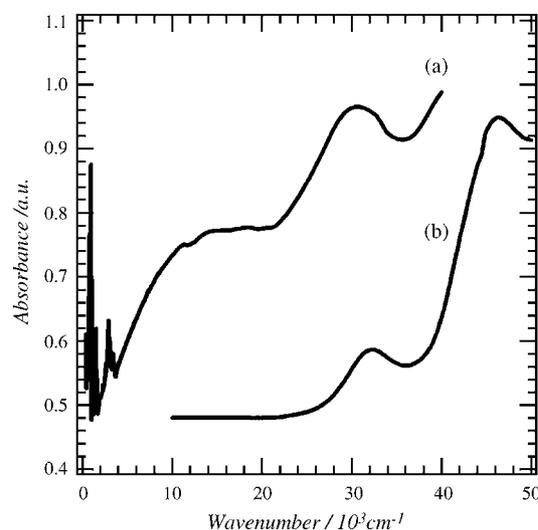
Fig. 1. Electronic spectra of salt (a) **3** in a KBr disk and (b) solution spectrum of $(H^+)_3[PMo_{12}O_{40}]^{3-}$ in CH_3CN [85].

to Mo ion splits the d-orbitals to t_{2g}- and e_g-orbitals, whose energy separation was usually larger than 10×10^3 cm^{-1}, the low energy absorption in salts **1–6** was assigned to the intervalence transition from the Mo^V to Mo^{VI} within the cluster and the d–d transitions of the Mo^V octahedron [92,93]. Since the terminal Mo–O distance (d_t) of $[PMo_{12}O_{40}]$ cluster was shorter than those of inner (d_a) and bridging Mo–O distances (d_b), it can be suggested that the $[MoO_6]$ octahedra were rather too distorted to cause further splitting of the d-orbitals. Therefore, complex and broad electronic absorption bands were observed at energies below $\sim 18 \times 10^3$ cm^{-1} [35–37].

The formation of one-electron reduced $[PMo_{12}O_{40}]^{4-}$ clusters was confirmed by recording the temperature dependent magnetic susceptibilities of salts **1–6** (see Section 4.4). From the appearance of the intervalence transition at $\sim 8 \times 10^3$ cm^{-1} in the electronic spectra, one 4d electron in the $[PMo_{12}O_{40}]^{4-}$ cluster appears delocalized over the cluster at room temperature [35–37]. A polycrystalline sample of salt **2**, displays a Lorentzian-type EPR spectrum at $g = 1.946$ with line-width (ΔH) of 4.73 mT at 5 K [85]. The g-value and ΔH at 80 K were 1.945 and 8.17 mT, respectively. The intensity of EPR signals of salt **2** followed the Curie–Weiss law, which was consistent with the temperature dependent magnetic susceptibility. Fig. 2 shows the temperature dependent line-width ΔH of salt **2**. Although the g-values showed temperature independent behavior from 4 to 100 K, an abrupt enhancement of ΔH values was observed by increasing of the temperature at around 60 K. The magnitude of ΔH at 100 K (12.89 mT) was about three times larger than that at 50 K (4.00 mT), and the change in ΔH has been discussed from a motional freedom of one $S = 1/2$ spin on the reduced $[PMo_{12}O_{40}]^{4-}$ cluster. The temperature dependent ΔH values of the Keggin cluster were composed of the sum of temperature independent ΔH_0 and temperature dependent ΔH_T as expressed in Eq. (1), where the ΔH_T term is proportional to the hopping frequency (ν_T) of $S = 1/2$ spin between the nearest-neighboring Mo sites
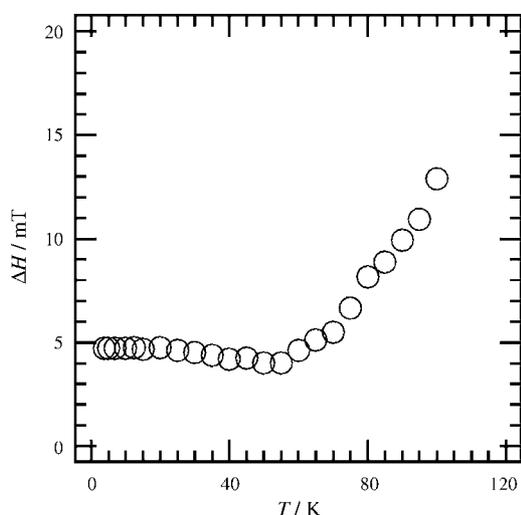
Fig. 2. Temperature dependent EPR spectra of salt **2**. Temperature dependent ΔH value in the temperature range from 4 to 100 K [85].

[94,95]:

$$\Delta H = \Delta H_0 + \Delta H_T = \Delta H_0 + C\nu_T \qquad (1)$$

The ν_T term can be further expressed by Mott's hopping frequency as [96,97]:

$$\nu_T = \nu_0 \exp(-2\alpha R) \exp\left(\frac{-E_{th}}{k_B T}\right) \qquad (2)$$

where α, R, and E_{th} were tunneling factor, nearest neighboring Mo–Mo distance, and activation energy of spin dynamics, respectively. Since the ν_0, α, and R are constants, the $\ln \Delta H$ versus T^{-1} plots yield the E_{th} of spin dynamics within the reduced $[PMo_{12}O_{40}]^{4-}$ cluster. The E_{th} value was 0.015 eV for salt **2** in the temperature range from 60 to 120 K, a similar value to those previously reported [35]. Thus the unpaired electron is localized at a specific Mo^V site below temperatures of 60 K, while the spin had a motional freedom between the twelve Mo sites above 60 K. Therefore it follows that although the $[PMo_{12}O_{40}]^{4-}$ clusters crystallize in the lattice, it is not possible according the crystal periodicity, to locate each spin or electron of $[PMo_{12}O_{40}]^{4-}$ due to delocalization over the entire framework.

4.3. Crystal structures of mixed-valence $[PMo_{12}O_{40}]^{4-}$ salts

The supramolecular cation structures were formed as a result of N–H$^+\sim$O hydrogen-bonding interactions between the ammonium moiety of the protonated PPD derivatives and oxygen atoms of crown ethers. The PPD overall shape and protonation state depends on the combination of PPD derivatives and crown ethers. Since the one-electron reduced $[PMo_{12}O_{40}]^{4-}$ anions were introduced into the crystals, the electrostatic interactions between the supramolecular cations and $[PMo_{12}O_{40}]^{4-}$ should be the dominant forces directing the structure of the crystal lattice. Therefore, the overall cation shape should influence the packing structures of $[PMo_{12}O_{40}]^{4-}$ anions in the crystals. The spin or electron on the cluster can be located at many sites, due

to a motional freedom with low activation energy at room temperature, or delocalized over the clusters in the crystal space according to the supramolecular cation structures.

4.3.1. Hydrogen-bonding supramolecular cation structures

The molecular-assemblies of protonated PPD–crown ethers in salts **1**–**6** are quite distinct from each other (Fig. 3). However, the hydrogen-bonded interactions between the –NH$_3^+$ moiety of PPD and the crown ether oxygen atoms are a common feature of the supramolecular cation structures. In contrast, the affinity between the oxygen atoms of the crown ether and the neutral –NH$_2$ group is low [63–66]. Therefore, sandwich-type cation structures of $(H2PPD^{2+})([12]crown-4)_2$, $(H2PPD^{2+})([18]crown-6)_2$, and $(TM-H2PPD^{2+})([18]crown-6)_2$ were observed in the di-protonated H2PPD^{2+} derivatives in salts **1**, **3**, and **5** (Fig. 3a, c, and e), in which oxygen atoms of upper and lower crown ether molecules interact with the two –NH$_3^+$ groups of H2PPD^{2+} and TM-H2PPD^{2+} through the N–H$^+\sim$O hydrogen bonds. On the other hand, the protonated state of PPD in salts **2**, **4**, and **6** was the mono-protonated HPPD$^+$ rather than the dicationic H2PPD^{2+} which provided the 1:1 (HPPD$^+$)(crown ether) supramolecular cation structure. For example, the hydrogen-bonding interactions between the five oxygen atoms of [15]crown-5 and the HPPD$^+$ occurred at the –NH$_3^+$ group of HPPD$^+$; the upper and lower nitrogen-sites of HPPD$^+$ in Fig. 3b were –NH$_2$ and –NH$_3^+$ moiety, respectively.

Both HPPD$^+$ and H2PPD^{2+} cations coexisted as HPPD$^+$([18]crown-6) and sandwich-type H2PPD^{2+}([18]crown-6)$_2$ in salt **3** (Fig. 3c). The dihedral angles between mean π-plane of the phenyl-ring and mean O6-plane of [18]crown-6 were about 100°. Therefore, the long axis of HPPD$^+$ and H2PPD^{2+} molecules were almost normal to the O6-plane of [18]crown-6. Both the HPPD$^+$ and H2PPD^{2+}, which were present as a Brønsted acid–base equilibrium during the crystallization, were introduced into the crystal and facilitated the closely packed structures of cations and anions.

The introduction of substituents such as 2-nitro (NO$_2$-PPD), 2,3,5,6-tetramethyl (TM-PPD), and *N*-phenyl (*N*-Ph-PPD) into the PPD molecule modified the overall supramolecular cation structures and intermolecular interactions in salts **4**–**6**. The formation of a supramolecular cation occurred at one ammonium moiety of NO$_2$-HPPD$^+$ against the [18]crown-6 molecule, consistent with the formation of monoprotonated 3-nitro-4-amino-anilinium (NO$_2$-HPPD$^+$) in salt **4** (Fig. 3d). Effective N–H$^+\sim$O hydrogen-bonding interactions were observed between the –NH$_3^+$ moiety of NO$_2$-HPPD$^+$ and oxygen atoms of [18]crown-6. In salt **4**, two kinds of crystallographically independent (NO$_2$-HPPD$^+$)([18]crown-6) units (**A** and **B**) interact in an anti-parallel dimer arrangement to reduce the dipole–dipole interaction between the NO$_2$-HPPD$^+$ molecules, which formed a pseudo-sandwich-type supramolecular cation structure (Fig. 3d). Therefore, it appears that the dipole–dipole interaction between two NO$_2$-HPPD$^+$ molecules is a dominant factor in determining the local supramolecular cation assembly of $[PMo_{12}O_{40}]^{4-}$ salt.

The stoichiometry of salt **5**, $(TM-H2PPD^{2+})_2(TM-PPD)_2([18]crown-6)_2[PMo_{12}O_{40}]^{4-}(CH_3CN)_2$, was different
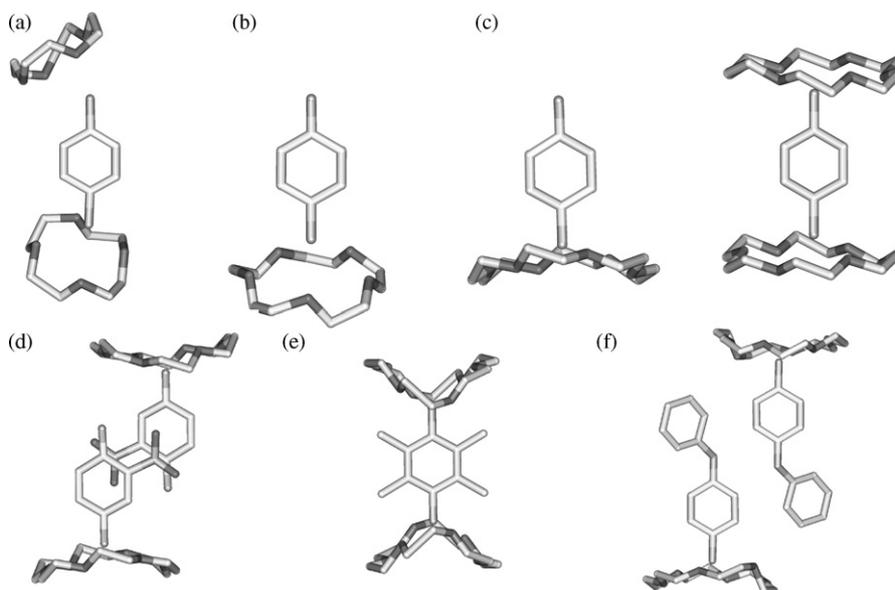
Fig. 3. Supramolecular cationic structures in salts **1**–**6**. (a) Largely deformed sandwich-type H2PPD^{2+}([12]crown-4)$_2$ structure in salt **1** viewed normal to π-plane of H2PPD^{2+}. (b) HPPD$^+$([15]crown-5) structure in salt **2**. (c) Mono-cationic HPPD$^+$([18]crown-6) (left) and dicationic H2PPD^{2+}([18]crown-6) (right) in salt **3**. (d) Dimer arrangement of mono-cationic (NO$_2$-HPPD$^+$)([18]crown-6) in salt **4**. (e) Sandwich-type dicationic (TM-H2PPD^{2+})([18]crown-6)$_2$ in salt **5**. (f) Dimer arrangement of mono-cationic (N-Ph-HPPD$^+$)([18]crown-6) in salt **6**.

from those of salts **4** and **6**. Neutral TM-PPD molecules were introduced into the crystal without the formation of hydrogen-bonded interactions to [18]crown-6. Two [18]crown-6 molecules interact with the upper and lower side of the –NH$_3^+$ moieties of di-protonated TM-H2PPD^{2+}, which formed the sandwich-type (TM-H2PPD^{2+})([18]crown-6)$_2$ supramolecular cation (Fig. 3e). The conformation of two [18]crown-6 molecules in salt **5** was relatively different from that of (H2PPD^{2+})([18]crown-6)$_2$ in salt **3**. The methyl substituents of TM-PPD molecule caused quite large steric repulsion between the methyl groups of TM-H2PPD^{2+} and [18]crown-6 molecules, resulting in largely deformed [18]crown-6 molecules, which increased the overall cation size.

The introduction of phenyl substituent into one N-site of PPD molecule increased the size of cation along the long axis of PPD, which also prevented the formation of sandwich-type supramolecular cation structure through the hydrogen-bonding interactions with [18]crown-6 molecule. One –NH$_3^+$ moiety of mono-protonated N-Ph-HPPD$^+$ interacts with a [18]crown-6 molecule through the N–H$^+\sim$O hydrogen-bonding interactions, in which the π-plane of HPPD$^+$ moiety was almost normal to the mean O6-plane of [18]crown-6. The introduction of a bulky phenyl substituent into the HPPD$^+$ molecule did not affect the formation of hydrogen-bonding supramolecular cation of (N-Ph-HPPD$^+$)([18]crown-6). Two nearest-neighboring (N-Ph-HPPD$^+$)([18]crown-6) units formed a weak dimer structure, in which the π-plane of N-substituted phenyl group existed beside the [18]crown-6 molecule.

The strengths of the N–H$^+\sim$O hydrogen-bonding interactions of the cations in salts **1**–**6** were evaluated from the average N–O distance ($d_{N–O}$) between the –NH$_3^+$ group of HPPD$^+$ or H$_2$PPD^{2+} and the crown ether oxygen atoms. The

average $d_{N–O}$ distances in salts **1**, **2**, **3**, **4**, **5**, and **6** were 2.89, 2.88, 2.92, 2.91, 2.89, and 2.92 Å, respectively. Thus the hydrogen-bonded supramolecular cationic structures in salts **1**–**6** were constructed from N–H$^+\sim$O hydrogen-bonding interactions where the hydrogen-bonded interactions are roughly of the same order of magnitude [98,99] (Fig. 3).

4.3.2. Packing structures of cations and anions in the crystals

The P–P distance ($d_{P–P}$) between the nearest-neighboring [PMo$_{12}$O$_{40}$]$^{4-}$ clusters was evaluated as a structural parameter to indicate the magnitude of the inter-cluster interactions. Since the size of the [PMo$_{12}$O$_{40}$] cluster was about 14 Å, a $d_{P–P}$ value around 14 Å is in the range of a van der Waals interaction [100]. Table 2 summarizes $d_{P–P}$ values of less than 16 Å in salts **1**–**6**.

The sandwich-type H$_2$PPD^{2+}([12]crown-4)$_2$ cation is the most compact supramolecular cation structure of the structures **1**–**6**, which is arranged between the [PMo$_{12}$O$_{40}$]$^{4-}$ clusters along the a- and b-axis. The effective intermolecular interactions between cations and anions were not observed within

Table 2
Interatomic P–P distances (Å) between [PMo$_{12}$O$_{40}$]$^{4-}$ units in salts **1**–**6**

Direction	**1**	**2**	**3**	**4**	**5**	**6**
a	12.1(7)	13.6(6)	14.2(1)	13.16(7)	–	–
b	13.1(6)	14.6(6)	14.6(1)	–	–	–
c	14.4(7)	–	14.9(1)	–	–	15.092(3)
−a + b	13.7(4)	15.6(4)	–	–	–	–
a + b	–	–	–	–	14.4(2)	–
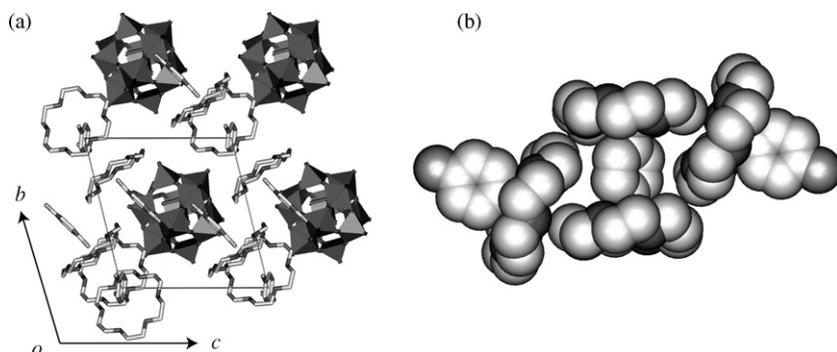
Fig. 4. Crystal structure of salt **3**. (a) Unit cell viewed along the *a*-axis. (b) Supramolecular cation assembly of $(H2PPD^{2+})([18]crown-6)_2$–$[HPPD^+([18]crown-6)]_2$ [85].

the limit of van der Waals interactions [100]. Within the *ab*-plane, a two-dimensional (2D) layer of $[PMo_{12}O_{40}]^{4-}$ clusters was observed, and the most dense cluster packing was observed in salt **1**. In salt **2**, two kinds of crystallographically independent $(HPPD^+)([15]crown-5)$ cations **A** and **B** units were observed. The $(HPPD^+)([15]crown-5)$ cations **A** and **B** formed an anti-parallel dimer arrangement around the center of the unit cell whereby alternate arrangements of $(HPPD^+)([15]crown-5)$ **A**- and **B**-units were observed along the *a*- and *b*-axis, which formed the cation layer within the *ab*-plane. The cation dimer was surrounded by eight nearest-neighboring $[PMo_{12}O_{40}]^{4-}$ clusters in the crystal. In the case of salt **3**, the sandwich-type $(H_2PPD^{2+})([18]crown-6)_2$ cations were observed on the lattice points (Fig. 4a), while two mono-protonated $(HPPD^+)([18]crown-6)$ cations existed around the center of the unit cell. Weak intermolecular interactions were observed between the sandwich-type di-protonated $(H2PPD^{2+})([18]crown-6)_2$ and monoprotonated $(HPPD^+)([18]crown-6)$ (Fig. 4b). Here, two $(HPPD^+)([18]crown-6)$ units are arranged around the axis of the sandwich-type $(H2PPD^{2+})([18]crown-6)_2$ cation and two [18]crown-6 molecules are inter-digitated into the space around the $H2PPD^{2+}$ dication (Fig. 4b).

In the case of **4**, a two-dimensional $[PMo_{12}O_{40}]^{4-}$ arrangement was observed in the *ab*-plane, in which the inter-cluster interaction along the *a*-axis ($d_{P-P} = 13.6$ Å) was stronger than

that along the *b*-axis ($d_{P-P} = 14.6$ Å). Therefore, the organization of the $[PMo_{12}O_{40}]^{4-}$ clusters along the *a*-axis represents a strong inter-cluster interaction in salt **4**. The supramolecular cations of $(NO_2-HPPD^+)([18]crown-6)$ formed a dimer structure through the dipole–dipole interaction of NO_2-HPPD^+ cations. The dimer arrangements within the *ab*-plane prevented the inter-cluster interaction along the *c*-axis, and the alternate arrangement of cations and anions along the *c*-axis formed the layer structure in salt **4** (Fig. 5a). Within the cation layer, a 90° twisted arrangement of $(NO_2-HPPD^+)_2([18]crown-6)_2$ dimers was observed along the *a*-axis (Fig. 5b), in which the π-planes of the NO_2-HPPD^+ cation were stacked through the π–π interactions along the *a*-axis. Since the mean inter-planar distances between the planes defined by the six carbon atoms forming the aromatic rings for the intra-dimer and inter-dimer units of NO_2-HPPD^+ cations were 3.2 and 3.6 Å, respectively, the π–π interactions within the dimer were stronger than the inter-dimer interactions.

The most effective inter-cluster interaction in salt **5** was observed along the *a* + *b*-axis with d_{P-P} of 14.4 Å within the range of van der Waals contact [100]. Since all other interactions were not effective in the crystal, the one-dimensional inter-cluster interactions provide the driving force for the ordering seen in the lattice of **5** (see Fig. 6). The cationic structures of salt **5** were constructed from both the di-protonated sandwich-type $TM-H2PPD^{2+}([18]crown-6)_2$ supramolecular cation and
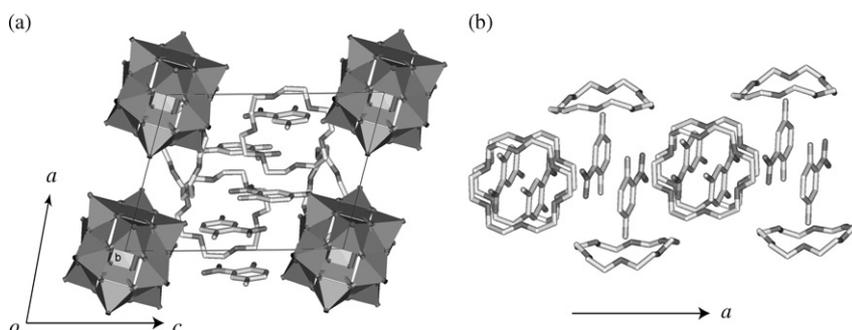
Fig. 5. Crystal structure of salt **4**. (a) Unit cell viewed along the *b*-axis. Hydrogen atoms were omitted for clarity. (b) Dimer arrangement of $(NO_2-HPPD^+)([18]crown-6)$ cations along the *a*-axis.
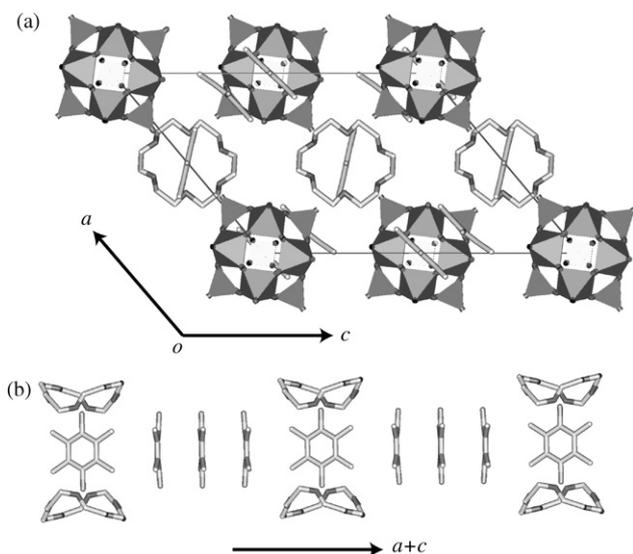
Fig. 6. Crystal structure of salt **5**. (a) Unit cell viewed along the *b*-axis. Hydrogen atoms were omitted for clarity. (b) Supramolecular cation of (TM-H2PPD^{2+})([18]crown-6) and trimer units of TM-PPD molecules along the *a* + *c*-axis.

TM-PPD–TM-H2PPD^{2+}–TM-PPD trimer. The neutral TM-PPD molecules were introduced into the crystal, which formed a trimer structure through the π–π interactions of TM-PPD and TM-H2PPD^{2+} molecules with mean inter-planar distance of 3.7 Å. TM-PPD trimers were arranged beside the π-plane of TM-H2PPD^{2+} dication along the *a* + *c*-axis, which filled the empty space of the ionic lattice between the (TM-H2PPD^{2+})([18]crown-6)$_2$ cations and [PMo$_{12}$O$_{40}$]$^{4-}$ anions.

Large supramolecular cations of (*N*-Ph-HPPD$^+$)([18]crown-6) in salt **6** completely disrupted the effective inter-cluster interactions within the crystal (see Fig. 7a). Since the shortest $d_{P–P}$ value (15.09 Å) along the *c*-axis was ca. 1 Å longer than the van der Waals contacts, the [PMo$_{12}$O$_{40}$]$^{4-}$ clusters were effectively isolated from each other. Instead, weakly bounded dimer units of (*N*-Ph-HPPD$^+$)([18]crown-6) filled the interstitial voids between the [PMo$_{12}$O$_{40}$]$^{4-}$ clusters, and each dimer was twisted at 90° along the *a*–*b*-axis without the effective intermolecular interactions (Fig. 7b).
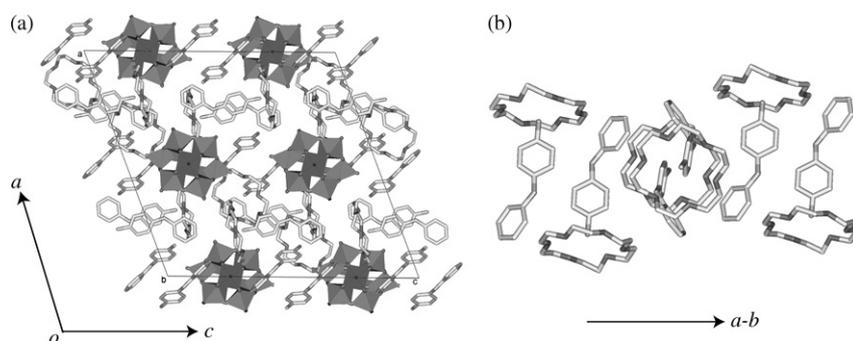
Fig. 8 summarizes the packing structures of the [PMo$_{12}$O$_{40}$]$^{4-}$ cluster anions within the *ab*-plane for salts **1**–**6** viewed along the *c*-axis. From the diameter of [PMo$_{12}$O$_{40}$]$^{4-}$ cluster and van der Waals radius of oxygen atom, a $d_{P–P}$ distance less than 14 Å corresponds to the effective inter-cluster interaction in the crystal.

The most dense packed arrangement of [PMo$_{12}$O$_{40}$]$^{4-}$ cluster anions of all salts **1**–**6** was found to be in the *ab*-plane of salt **1**, whose $d_{P–P}$ distances along the *a*- and −*a* + *b*-axis were 12.1 and 13.7 Å, respectively. The one-dimensional [PMo$_{12}$O$_{40}$]$^{4-}$ chain along the *a*-axis was connected through the inter-cluster interaction along the −*a* + *b*-axis, forming the two-dimensional layer within the *ab*-plane. The small and compact supramolecular cation structure of (H2PPD^{2+})([18]crown-6)$_2$ were densely packed in the space between the [PMo$_{12}$O$_{40}$]$^{4-}$ anions. Since the inter-cluster distance of salt **2** along the *a*-axis ($d_{P–P} = 13.6$ Å) was less than the van der Waals contact, the one-dimensional [PMo$_{12}$O$_{40}$]$^{4-}$ arrangement along the *a*-axis was the also an effective inter-cluster interaction. However, the most effective inter-cluster distance of salt **2** along the *a*-axis was 1.5 Å longer than that in salt **1**, suggesting that the packing density of the clusters in salt **2** was decreased by increasing of the size of crown ether from [12]crown-4 to [15]crown-5.

Although the most effective inter-cluster interaction of salt **3** was observed along the *a*-axis, the $d_{P–P}$ distance of 14.2 Å was longer than the van der Waals contact of [PMo$_{12}$O$_{40}$]$^{4-}$ clusters. The inter-cluster distances in salt **3** was enough longer than those in salt **1**, which suggested the isolated arrangement of Keggin clusters. Thus it can be seen that the relatively large size of [18]crown-6 molecules separated the [PMo$_{12}$O$_{40}$]$^{4-}$ clusters in salt **3**.

The most effective inter-cluster interaction of salt **4** was observed along the *a*-axis with $d_{P–P}$ of 13.16 Å within the limit of van der Waals contact [100]. Since the other $d_{P–P}$ distances along the *b*- and *c*-axis were ca. 3 Å longer than the inter-cluster interaction along the *a*-axis, the one-dimensional [PMo$_{12}$O$_{40}$]$^{4-}$ chain along the *a*-axis was the dominant interaction in the crystal. The $d_{P–P}$ distance in salt **4** was ca. 1 Å longer than that in salt **1** and similar to that of salt **2**. The supramolecular cation structures of (NO$_2$-HPPD$^+$)([18]crown-6), which had the dipole–dipole and π–π stacking interactions, yielded a relatively dense packing of the cations and anions in the crystal.

Fig. 7. Crystal structure of salt **6**. (a) Unit cell viewed along the *b*-axis. Hydrogen atoms were omitted for clarity. (b) Supramolecular cation arrangement of (*N*-Ph-HPPD$^+$)([18]crown-6) along the *a*–*b*-axis.
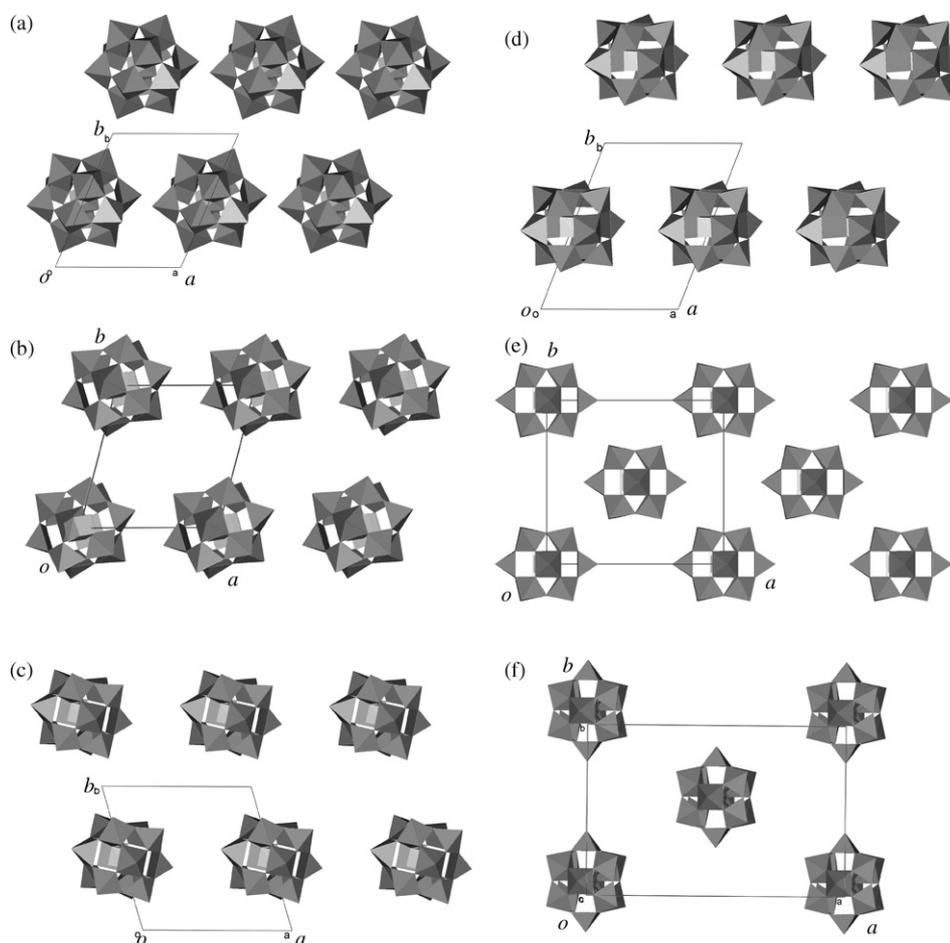
Fig. 8. Packing structures of $[PMo_{12}O_{40}]^{4-}$ within the *ab*-plane in salts (a) **1**, (b) **2**, (c) **3**, (d) **4**, (e) **5**, and (f) **6** viewed along the *c*-axis.

Since the shortest d_{P-P} distance of 14.4 Å for salt **5** along the $a + b$-axis was longer than the van der Waals contact, each $[PMo_{12}O_{40}]^{4-}$ cluster was isolated from each other. The largely deformed [18]crown-6 molecules in (TM-H2PPD^{2+})([18]crown-6)$_2$ cations increased the cation size, which also allowed the introduction of the neutral TM-PPD molecules into the crystal lattice to fill the empty space. Therefore, the inter-cluster distances within the *ab*-plane were quite significantly elongated in comparison with those in salts **1–4**. Similarly, the effective d_{P-P} distances of salt **6** (>15 Å) were not observed within the limit of van der Waals contacts [100], suggesting that the $[PMo_{12}O_{40}]^{4-}$ arrangement of the cluster anions effectively isolations them from each other within the crystal lattice. This means that introduction of the much larger supramolecular cations, (TM-H2PPD^{2+})([18]crown-6)$_2$ and (*N*-Ph-HPPD^{+})([18]crown-6), acts to isolate the $[PMo_{12}O_{40}]^{4-}$ clusters anions in **5** and **6**.

4.4. Magnetic susceptibilities of [PMo$_{12}$O$_{40}$]$^{4-}$ salts

Fig. 9a and b shows the $\chi_{mol}T$ versus T plots of salts **1–3** and salts **4–6**, respectively, in the temperature range from 2 to 300 K. The temperature dependent magnetic susceptibilities of salts **1–6** were similar to each other, in which the

$\chi_{mol}T$ versus T plots of all salts were in accordance with the Curie–Weiss behavior [101]. The Curie constant of salt **1** (0.258 emu K mol^{-1}) was slightly decreased from the calculated Curie constant of 0.355 emu K mol^{-1} with $g = 1.945$, while the $C = 0.325$–0.351 emu K mol^{-1} of salts **2–6** was similar to the calculated Curie constant of 0.355 emu K mol^{-1}. The suppression of magnetic susceptibility in salt **1** may be due to (i) spin-orbital coupling of the distorted Mo^{V} octahedron or (ii) antiferromagnetic interaction between $[PMo_{12}O_{40}]^{4-}$ clusters.

The antiferromagnetic interactions between $[PMo_{12}O_{40}]^{4-}$ clusters are also expected to reduce the *C*-value of salt **1**. In the crystal, the most dense packing of $[PMo_{12}O_{40}]^{4-}$ clusters were observed in salt **1** along the *a*-axis. The short inter-cluster distance in salt **1** should also allow an increase in the magnetic exchange interactions between the $[PMo_{12}O_{40}]^{4-}$ clusters units. Although the LUMO coefficients at terminal oxygen atoms of Keggin structure are quite small [102,103], the inter-cluster antiferromagnetic exchange energy is expected to reduce the magnetic susceptibility of salt **1** so the possibility of a spin-orbital coupling of the Mo^{V} octahedron within the cluster remains. The magnitude of spin-orbital coupling constant for the second and third transition mental ions is usually larger than that for the first transition metal ions due to the d-electron broadening, which decreases the absolute magnitude of magnetic susceptibility. Table 3 summarizes Curie constant (*C*), the aver-
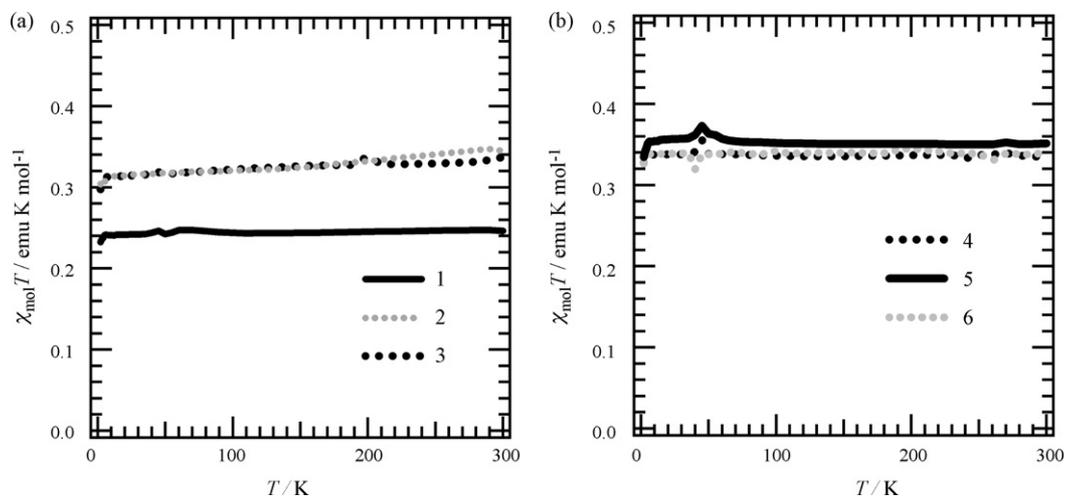
Fig. 9. The $\chi_{mol}T$ vs. T plots of (a) salts **1–3** [85] and (b) salts **4–6** in polycrystalline samples. The χ_{mol} of salts **1–6** per one $[PMo_{12}O_{40}]^{4-}$ cluster was plotted in figure.

Table 3
Curie constant and average Mo–O distances[a] in salts **1–6**

	1	**2**	**3**	**4**	**5**	**6**
C (emu K mol^{-1})	0.258	0.322	0.325	0.338	0.351	0.341
d_t (Å)	1.66	1.65	1.66	1.66	1.66	1.66
d_b (Å)	1.90	1.90	1.89	1.90	1.91	1.90
d_a (Å)	2.39	2.48	2.45	2.47	2.48	2.57

[a] The shape of $[MoO_6]$ octahedron was evaluated from Mo–O distances of terminal Mo–O (d_t), bridging Mo–O–Mo (d_b), and anionic Mo–PO$_4^{3-}$ (d_a).

age Mo–O distances of terminal Mo–O (d_t), bridging Mo–O–Mo (d_b), and anionic Mo–PO$_4^{3-}$ (d_a) in $[MoO_6]$ octahedron.

The distortion of $[MoO_6]$ octahedron was evaluated from Mo–O distances of d_t, d_b, and d_a. In salt **1**, the average distances of d_t, d_b, and d_a were 1.66, 1.90, and 2.39 Å, respectively, which were within the same range of previously reported reduced Keggin structures of $[Fe(C_5Me_5)_2]_4[PMo_{12}O_{40}]^{4-}$ and

(tetrathiafulvalene)$_6$(tetraethylammonium$^+$)(H$^+$)$[PMo_{12}O_{40}]^{4-}$ [23,24]. Since the terminal d_t of salt **1** was ca. 0.3 and 0.7 Å shorter than the bridging d_b and anionic d_a, the $[MoO_6]$ octahedron was distorted from an ideal octahedron. Although the lengths of d_t and d_b for salts **1–6** were observed within the similar range, the length of d_a for salt **1** (2.39 Å) was about 0.1 Å shorter than those of salts **2–6** (2.45–2.57 Å). Therefore, the structural distortion of $[MoO_6]$ octahedron for salt **1** was smaller than those of salts **2–6**. Both the spin-orbital coupling on Mo^V octahedron and antiferromagnetic interaction between $[PMo_{12}O_{40}]^{4-}$ clusters play an important role to reduce the absolute magnitude of magnetic susceptibility in the salt **1**.

5. Inorganic polyoxometalate frameworks as crowns

POM clusters themselves can be seen as excellent crown-type ligands due to their structured and well-organized metal oxo framework [104–106]. The classic example of a cluster with such a feature is the Pressler-anion, $[NaP_5W_{30}O_{110}]^{14-}$ $\{P_5W_{30}\}$ [107]. The fivefold symmetry of this anion is completed by the linkage of five $\{PW_6\}$ groups and the central
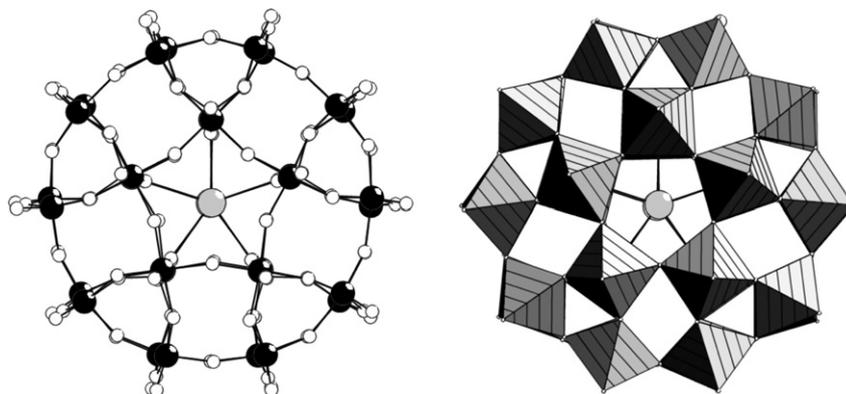
Fig. 10. Structure of the $[NaP_5W_{30}O_{110}]^{14-}$ anion, $\{P_5W_{30}\}$ [107]. A ball and stick representation is shown on the left-figure and a polyhedral representation on the right-figure. The central sodium ion is depicted as a large grey sphere.
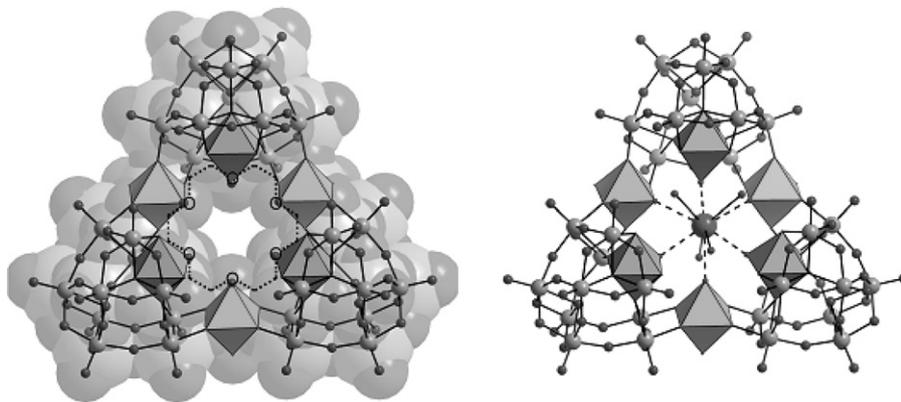
Fig. 11. (Left) Comparative illustration of the $\{W_{36}\}$ cluster framework $[H_{12}W_{36}O_{120}]^{12-}$ and the 18-crown-6 structure (show to scale) [112,113]. W and O atoms shown as light and dark spheres, respectively, with the crown-ether superimposed on O atoms forming the 'cavity' of the cluster. The ball and stick structure is also superimposed on the space filling CPK representation, along with a polyhedral representation of the six W units that provide the 'crown' coordinating O atoms. (Right) The same ball and stick/polyhedral structure but this time showing the complexed potassium ion and the ligated water molecules within the cavity representing the overall $\{(H_2O)_4K \subset [H_{12}W_{36}O_{120}]\}^{11-}$ complex.

sodium ion lies in the center of a plane defined by the oxygen atoms of the phosphate groups (see Fig. 10). It appears that this kinetically inert (on the NMR timescale) sodium ion is essential for the construction of the cluster [108]. The presence of the sodium cation reduces the overall anion symmetry from D_{5h} to C_{5v}. The $\{P_5W_{30}\}$ anion is robust and the central Na^+ can be replaced by other cations of similar size, e.g. Ca^{2+}, most Ln^{III}, and U^{IV} under hydrothermal conditions [109–111]. These types of POM-based crown-like moieties clearly can be exploited so they can act as inorganic crowns for the complexation of cations and supramolecular cations.

Although the cations in the Pressler anion are not so rapidly easily interchanged, a wide variety of other systems are know that can accommodate a range of cations. For example the isopolyoxotungstate cluster, $[H_{12}W_{36}O_{120}]^{12-}$ which has a tri-angular topology, can bind cations [112]. In analogy to an [18]crown-6 with six oxygen-based receptor sites on a ring, the $[H_{12}W_{36}O_{120}]^{12-}$ cluster can form alkali and alkaline earth metal complexes $\{M \subset W_{36}\}$ ($M = K^+$, Rb^+, Cs^+, NH_4^+, Sr^{2+} and Ba^{2+}, see Fig. 11) [113]. Therefore, if the cation can also be exchanged for R-NH_3^+ cation species, as demonstrated here, then it will be possible to design new types of architecture where the crown-like host is also a POM cluster. This then offers great potential for the design of electronically interesting materials where the 'crown' framework can also localize or delocalize unpaired electrons. Coupling this with electronically interest-ing R-NH_3^+ cation species offers real potential to design new nanoscale materials and devices [112,113].

POMs can also be used to construct spherical capsules with well-defined pores has been spectacularly demonstrated using POM-based building blocks. POMs represent a vast range of clusters based on MO_x units which form structures with nucle-arities ranging from 6 to 368 atoms (M mostly refers to Mo, W, V and x can be 4, 5, 6 or 7) [11,114]. Interestingly, even comparably small clusters can have remarkable physical prop-erties as a result of encapsulating electronically or chemically active moieties [115,116]. However, some of the most inter-esting cluster types for nanoscience are those with ring and

spherical shapes comprising of pentagonal $\{(Mo)Mo_5\}$ build-ing blocks [11]. For instance, ultra large molybdenum clusters of the wheel and spherical type with a variety of cavity sizes have been utilized in the design and investigation of supramolec-ular systems. In particular a system with a Mo-blue wheel, $\{Mo_{176}\} = Na^+{}_{(32-n)}[\{MoO_3\}_{176}(H_2O)_{63}(MeOH)_{17}H_n{}^+]$ with an inner cavity diameter of ca. 2.3 nm (see Fig. 12) was used to complex a tetrakis(4-aminophenyl)porphyrin. This was used to fabricate islands of isolated porphyrin on a surface and imaged using STM techniques [117]. All the spherical and approxi-mately icosahedral clusters have the form $[\{(pent)_{12}(link)_{30}\}]$, e.g. like $[\{(Mo)Mo_5O_{21}(H_2O)_6\}_{12}\{Mo_2O_4(ligand)\}_{30}]^{n-}$ with binuclear linkers where the 12 central pentagonal units span an icosahedron and the linkers are a distorted truncated icosahe-dron; the highly charged capsule with sulphate ligands and $n = 72$ was used very successfully. For instance, the truly nanoscale capsules (inner cavity diameter ca. 2.5 nm) allow different types of encapsulations, e.g. of well-structured large water assemblies (up to 100 molecules) with an 'onion' like layer structure enforced by the outer shell [11,114]. Most important, the capsules have 20 well-defined pores and the internal shell functionalities can be tuned precisely since the nature of the bidentate ligands can be varied (see Fig. 12). In the special case of binuclear $\{Mo_2^VO_4\}^{2+}$ linkers the pores are $\{Mo_9O_9\}$ rings with a crown ether function (diameters 0.6–0.8 nm) which can be reversibly closed, e.g. by guanidinium cations non-covalently interacting with the rings *via* formation of hydrogen bonds [118]. In a related smaller capsule with mononuclear linkers the $\{Mo_6O_6\}$ pores can get closed/complexed correspondingly by smaller potassium ions [119].

The most intriguing and exciting property of the highly negatively charged capsules is that they can mediate cation transfer from the solution to the inner nanocavity. Indeed, reaction of the above-mentioned highly charged capsule with different substrates/cations such as Na^+, Cs^+, Ce^{3+}, $C(NH_2)_3{}^+$, and $OC(NH_2)NH_3{}^+$ in aqueous solution leads to forma-tions/assemblies which exhibit well-defined cation separations *at*, *above*, or *below* the capsules channel-landscapes ('nano-ion
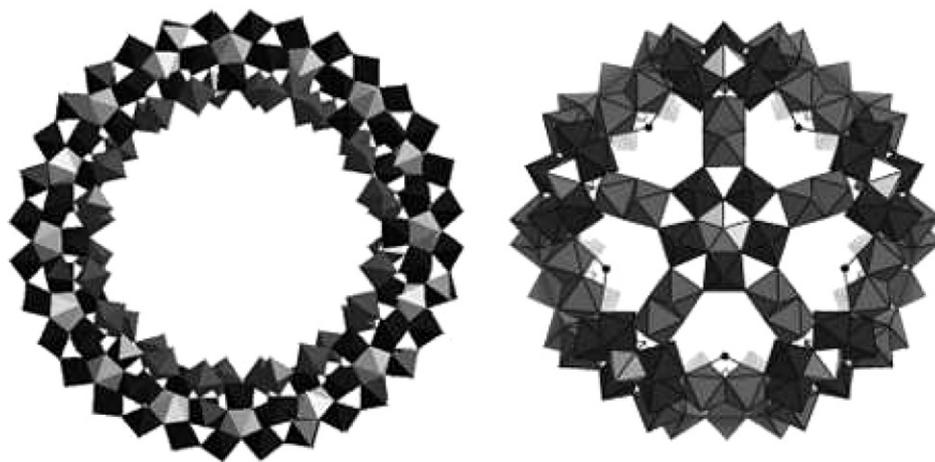
Fig. 12. Polyhedral representation of the $\{Mo_{176}\} = Na^{+}_{(32-n)}[\{MoO_3\}_{176}(H_2O)_{63}(MeOH)_{17}H_n^{+}]$ of the wheel cluster (left) and the $\{Mo_{132}\} = [\{(Mo)Mo_5O_{21}(H_2O)_6\}_{12}\{Mo_2O_4(SO_4)\}_{30}]^{72-}$ spherical cluster (right).

chromatograph' behavior) [120]. Taking this one step further a temperature-dependent equilibrium process that involves the uptake/release of Li^+ ions through the capsule pores has been observed: the porous capsule behaves as a semi-permeable inorganic membrane open for H_2O and small cations [121,122]. Furthermore, the 20 pores of the same capsule 'shut' by protonated urea as "stoppers", can be opened in solution thus allowing Ca^{2+} ion uptake while later closing occurs again [123]. As such these systems can show "pore gating" – just modeling biological ion transport – can illustratively be demonstrated: after initial cation uptake, subsequent cations are found hydrated above the pores due to a decrease of negative capsule charge [124].

In summary in this section we have seen how POM clusters of varying sizes can themselves be used as the supramolecular receptor. Therefore, this means that it is possible to extend the design principles presented in Sections 2–4 to replace the organic receptor with a POM based crown and combine the recognition and electronic properties.

6. Conclusions

Supramolecular cation structures between protonated *p*-phenylenediamine (PPD) derivatives of PPD and crown ethers were introduced into the one-electron reduced mixed-valence α-$[PMo_{12}O_{40}]^{4-}$ Keggin salts. The electron-transfer and proton-transfer processes between the electron-donor (proton-acceptor) of PPD derivatives and the electron-acceptor (proton-donor) of the $(H^+)_3[PMo_{12}O_{40}]^{3-}$ clusters occurred in the crystallization process. The cation structures of PPDs – crown ethers – $[PMo_{12}O_{40}]^{4-}$ assemblies were constructed from the hydrogen-bonding structural units between one or two ammonium moiety of PPDs and oxygen atoms of crown ethers. The Brønsted acid–base equilibrium and the formation of closely packed structures yielded a range of cationic structures and molecular-assemblies in $[PMo_{12}O_{40}]^{4-}$ salts. The most dense packed arrangement of $[PMo_{12}O_{40}]^{4-}$ was observed in the small size supramolecular cation of $(H2PPD^{2+})([12]crown4)_2$, in which one-dimensional $[PMo_{12}O_{40}]^{4-}$ chains were connected through the inter-chain interactions as two-dimensional

inorganic layers. Although inter-cluster interactions between $[PMo_{12}O_{40}]^{4-}$ anions were observed in other salts, the magnetic spin associated with each cluster was isolated with respect to each other in the solid state. By increasing the size of crown ethers, the magnitude of inter-cluster interactions decreased in the order of [12]crown-4, [15]crown-5, to [18]crown-6 because of the increasing of the cation volume in the crystals. The increasing of the size in PPD derivatives also elongated the inter-cluster distances, while the dipole–dipole and π-stacking interactions of NO_2-HPPD$^+$ molecules were also effective to facilitate the dense packing of the cations and anions. Although fundamentally speaking the materials were constructed using the electrostatic interaction between the one-electron reduced $[PMo_{12}O_{40}]^{4-}$ anion, and the supramolecular cations, the structures could be modulated significantly by changing the shape and size of the supramolecular cation. The cation size of $(H2PPD^{2+})([12]crown-4)_2$ can be seen to be a good fit in the formation of a closed-packing structure of $[PMo_{12}O_{40}]^{4-}$ tetravalent anions in the crystal. The nature of the one-electron reduced α-$[PMo_{12}O_{40}]^{4-}$ cluster anion, bearing one $S = 1/2$ spin, was confirmed by the temperature-dependent magnetic susceptibilities. Furthermore, the electronic absorption spectra revealed the intervalence optical transition between the pentavalent Mo^V and hexavalent Mo^{VI} ions within the cluster. In addition, temperature dependent EPR spectra of $(HPPD^+)_4([15]crown-5)_4[PMo_{12}O_{40}]^{4-}$ showed the delocalization of $S = 1/2$ spin on the cluster above 60 K. The localization–delocalization spin transition was observed at 60 K by temperature dependent line-width of the EPR spectra. The control of spin dynamics and intervalence electron-transfer within the reduced Keggin clusters has a potential to form novel electrical and magnetic materials of organic–inorganic hybrid molecular system.

In this work we have shown how the compartmentalization of the design process can lead to the crystal engineering of novel frameworks of supramolecular cations and cluster anions. Here the crucial consideration lies with size matching the inorganic cluster anion with the designable organic cation unit that itself is unit formed by supramolecular interactions [68–82].

Furthermore, the development of wholly inorganic supramolecular receptors provides a direct route to produce frameworks that combine the electronic and recognition properties into one molecular polyoxometalate building block. Further, by tuning the electronic structure of the framework it may even be possible to activate or deactivate cation binding leading to a possible switchable system. By combining many properties in one set of building blocks increases the possibility of realizing advanced functional materials that are robust, electronically interesting, functional and amenable to rational design.

Acknowledgements

Appendix A. Supplementary data

Supplementary data associated with this article can be found, in the online version, at doi:10.1016/j.ccr.2007.08.015.

References

[1] G. González-Moraga, Cluster Chemistry, Springer-Verlag, Berlin, 1993.
[2] P. Atkins, T. Overton, J. Rourke, M. Weller, F. Armstrong, Inorganic Chemistry, 4th ed., Oxford University Press, 2006.
[3] P.A. Cox, Transition Metal Oxides, Springer-Verlag, Berlin, 1992.
[4] D.-L. Long, E. Burkholder, L. Cronin, Chem. Soc. Rev. 36 (2007) 105.
[5] L. Cronin, C. Beugholt, A. Müller, J. Mol. Struct. Theochem. 500 (2000) 181.
[6] A. Müller, F. Peters, M.T. Pope, D. Gatteschi, Chem. Rev. 98 (1998) 239.
[7] D.-L. Long, L. Cronin, Chem. Eur. J. 12 (2006) 3699.
[8] J.J. Borrás-Almenar, E. Coronado, A. Müller, M. Pope (Eds.), Polyoxometalate Molecular Science, Kluwer Academic Publishers, London, 2001.
[9] M. Pope, A. Müller (Eds.), Polyoxometalate Chemistry From Topology via Self-Assembly to Applications, Kluwer Academic Publishers, London, 2001.
[10] T. Yamase, M. Pope (Eds.), Polyoxometalate Chemistry for Nano-Composite Design, Kluwer Academic Publishers, New York, 2002.
[11] L. Cronin, Compr. Coord. Chem. II 7 (2004) 1.
[12] A. Müller, P. Kögerler, C. Kuhlmann, Chem. Commun. 1997 (1997) 1437.
[13] A. Müller, P. Kögerler, A.W.M. Dress, Coord. Chem. Rev. 222 (2001) 193.
[14] A. Müller, C. Serani, Acc. Chem. Res. 32 (2000) 2.
[15] A. Müller, S. Roy, Coord. Chem. Rev. 245 (2003) 153.
[16] References were cited in I.V. Kozhevnikov, Chem. Rev. 98 (1998) 171.
[17] References were cited in N. Mizuno, M. Misono, Chem. Rev. 98 (1998) 199.
[18] References were cited in J.T. Rhule, C.L. Hill, D.A. Judd, Chem Rev. 98 (1998) 327.
[19] Y. Ishi, Y. Takenaka, K. Konishi, Angew. Chem. Int. Ed. Engl. 43 (2004) 2702.
[20] H. Abbas, A.L. Pickering, D. Long, P. Kögerler, L. Cronin, Chem. Eur. J. 11 (2005) 1071.
[21] M. Clemente-León, E. Coronado, C.J. Gómez-Garcia, C. Mingotaud, S. Ravaine, G. Romualdo-Torres, P. Delhaès, Chem. Eur. J. 11 (2005) 3979.

[22] L. Ouahab, D. Grandjean, M. Bencharif, Acta Crystallogr., Sect. C 47 (1991) 2670.
[23] L. Ouahab, M. Bencharif, A. Mhanni, D. Pelloquin, J.-F. Halet, O. Peña, J. Padiou, D. Grandjean, C. Garrigou-Lagrange, J. Amiell, P. Delhaes, Chem. Mater. 4 (1992) 666.
[24] P.L. Maguerès, L. Ouahab, S. Golhen, D. Grandjean, O. Pena, J.-C. Jegaden, C.J. Gómez-Garcia, P. Delhaès, Inorg. Chem. 33 (1994) 5180.
[25] C.J. Gómez-Garcia, L. Ouahab, C. Gimenéz-Saiz, S. Triki, E. Coronado, P. Delhaès, Angew. Chem. Int. Ed. Engl. 33 (1994) 223.
[26] J.R. Galan-Mascarós, C. Gimenéz-Saiz, S. Triki, J. Gómez-Garcia, E. Coronado, L. Ouahab, Angew. Chem. Int. Ed. Engl. 34 (1995) 1460.
[27] C. Bellitto, M. Bonamico, V. Fares, F. Federici, G. Righini, M. Kurmoo, P. Day, Chem. Mater. 7 (1995) 1475.
[28] E. Coronado, J.R. Galan-Mascarós, C. Gimenéz-Saiz, C.J. Gómez-Garcia, S. Triki, J. Am. Chem. Soc. 120 (1998) 4671.
[29] E. Coronado, J.R. Galan-Mascarós, C. Gimenéz-Saiz, C.J. Gómez-Garcia, L.R. Falvello, P. Delhaès, Inorg. Chem. 37 (1998) 2183.
[30] E. Coronado, C.J. Gómez-Garcia, Chem. Rev. 98 (1998) 273.
[31] E. Coronado, C. Giménez-Saiz, C.J. Gómez-Garcia, S.J. Capelli, Angew. Chem. Int. Ed. Engl. 43 (2004) 3022.
[32] M. Nyman, D. Ingersoll, S. Singh, F. Bonhomme, T.M. Alam, C.J. Brinker, M.A. Rodriguez, Chem. Mater. 17 (2005) 2885.
[33] E. Coronado, J.R. Galán-Mascarós, C. Giménez-Saiz, C.J. Gómez-García, E. Martínez-Ferrero, M. Almeida, E.B. Lopes, S.C. Capelli, R.M. Llusar, J. Mater. Chem. 14 (2004) 1867.
[34] D. Gatteschi, L. Pardi, A.L. Barra, A. Müller, J. Döring, Nature 354 (1991) 463.
[35] R.A. Prados, P.T. Meiklejohn, M.T. Pope, J. Am. Chem. Soc. 96 (1974) 1261.
[36] R.A. Prados, M.T. Pope, Inorg. Chem. 15 (1976) 2547.
[37] C. Sanchez, J. Livage, J.P. Launary, M. Fournier, Y. Jeannin, J. Am. Chem. Soc. 104 (1982) 3194.
[38] N. Suaud, A. Gaita-Ariño, J.M. Clemente-Juan, E. Coronado, Chem. Eur. J. 10 (2004) 4041.
[39] C. Baffert, J.F. Boas, A.M. Bond, P. Kögerler, D.-L. Long, J.R. Pilbrow, L. Cronin, Chem. Eur. J. 12 (2006) 8472.
[40] A.R. West, Basic Solid State Chemistry, John Wiley & Sons, 1988.
[41] N. Honma, K. Kusaka, T. Ozeki, Chem. Commun. 2002 (2002) 2896.
[42] H. Chiba, A. Wada, T. Ozeki, Dalton Trans. 2006 (2006) 1213.
[43] H. Zhang, L. Duan, Y. Lan, E. Wang, C. Hu, Inorg. Chem. 42 (2003) 8053.
[44] Y. Lu, Y. Xu, E. Wang, J. Lü, C. Hu, L. Xu, Cryst. Growth Des. 5 (2005) 385.
[45] X. Kong, Y. Ren, P. Zheng, Y. Long, L. Long, R. Huang, L. Zheng, Inorg. Chem. 45 (2006) 10702.
[46] X. Wang, Y. Guo, Y. Li, E. Wang, C. Hu, N. Hu, Inorg. Chem. 42 (2003) 4175.
[47] P. Zheng, Y. Ren, L. Lomg, R. Huang, L. Zheng, Inorg. Chem. 44 (2005) 1190.
[48] J.A.F. Gamelas, F.M. Santos, V. Felix, A.M.V. Cavaleiro, E. de M. Gomes, M. Belsley, M.G.B. Drew, Dalton Trans. (2006) 1197.
[49] C. Ritchie, E.M. Burkholder, D. Long, D. Adam, P. Kögerler, L. Cronin, Chem. Commun. 2007 (2007) 468.
[50] O. Nagao, Y. Sasaki, Acta. Cryst., Sect. B 35 (1979) 2387.
[51] R. Neier, C. Trojanowski, R. Mattes, J. Chem. Soc., Dalton Trans. 1995 (1995) 2521.
[52] A. Drljaca, M.J. Hardie, C.L. Raston, J. Chem. Soc., Dalton Trans. 1999 (1999) 3629.
[53] W.S. You, E.B. Wang, Y. Xu, Y. Li, L. Xu, Inorg. Chem. 40 (2001) 5648.
[54] W. You, E. Wang, Q. He, L. Xu, Y. Xing, H. Jia, J. Mol. Struct. 524 (2000) 133.
[55] W. You, E. Wang, L. Xu, Z. Zhu, Y. Gu, J. Mol. Struct. 605 (2002) 41.
[56] Y. Li, N. Hao, E. Wang, M. Yuan, C. Hu, N. Hu, H. Jia, Inorg. Chem. 42 (2003) 2792.
[57] X. Lu, B. Liu, S. Wang, C. Ye, Polyhedron 24 (2005) 2889.
[58] V. Shivaish, S.K. Das, Inorg. Chem. 44 (2005) 7313.
[59] V. Shivaiah, Inorg. Chem. Commun. 6 (2006) 1191.

[60] J.-M. Lehn, in: U. Anton (Ed.), Supramolecular Chemistry, VCH, Weinheim, 1995.
[61] J.W. Steed, J.L. Atwood, Supramolecular Chemistry, Wiley, Chichester, 2000.
[62] X. Wang, C. Qin, E. Wang, Z. Su, Y. Li, L. Xu, Angew. Chem. Int. Ed. Engl. 45 (2006) 7411.
[63] R.M. Izatt, J.S. Bradshaw, S.A. Nielsen, J.D. Lamb, J.J. Christensen, D. Sen, Chem. Rev. 85 (1985) 271.
[64] R.M. Izatt, K. Pawlak, J.D. Bradshaw, R.L. Bruening, Chem. Rev. 91 (1991) 721.
[65] E. Weber, J.L. Toner, I. Goldberg, F. Vögtle, D.A. Laidler, J.F. Stoddart, R.A. Bartsch, C.L. Liotta, in: S. Patai, Z. Rappoport (Eds.), Crown Ethers and Analogs, John Wiley & Sons, New York, 1989.
[66] G.W. Gökel, in: J.F. Stoddart (Ed.), Crown Ethers & Cryptands, RSC, Cambridge, 1994.
[67] Y.L. Ha, A.K. Chakraborty, J. Phys. Chem. 96 (1992) 6410.
[68] T. Nakamura, T. Akutagawa, K. Honda, A.E. Underhill, A.T. Coomber, R.H. Friend, Nature 394 (1998) 159.
[69] T. Akutagawa, Y. Nezu, T. Hasegawa, T. Nakamura, K. Sugiura, Y. Sakata, T. Inabe, A.E. Underhill, Chem. Commun. 1998 (1998) 2599.
[70] T. Akutagawa, T. Hasegawa, T. Nakamura, S. Takeda, T. Inabe, K. Sugiura, Y. Sakata, A.E. Underhill, Inorg. Chem. 39 (2000) 2645.
[71] T. Akutagawa, T. Hasegawa, T. Nakamura, S. Takeda, T. Inabe, K. Sugiura, Y. Sakata, A.E. Underhill, Chem. Eur. J. 7 (2001) 4902.
[72] T. Akutagawa, T. Hasegawa, T. Nakamura, T. Inabe, J. Am. Chem. Soc. 124 (2002) 8903.
[73] N. Takamatsu, T. Akutagawa, T. Hasegawa, T. Nakamura, T. Inabe, W. Fujita, K. Awaga, Inorg. Chem. 39 (2000) 870.
[74] T. Akutagawa, S. Nishihara, N. Takamatsu, T. Hasegawa, T. Nakamura, T. Inabe, J. Phys. Chem. B 104 (2000) 5871.
[75] T. Akutagawa, N. Takamatsu, K. Shitagami, T. Hasegawa, T. Nakamura, T. Inabe, J. Mater. Chem. 11 (2001) 2118.
[76] T. Akutagawa, A. Hashimoto, S. Nishihara, T. Hasegawa, T. Nakamura, J. Supra. Chem. 2 (2002) 175.
[77] T. Akutagawa, A. Hashimoto, S. Nishihara, T. Hasegawa, T. Nakamura, J. Phys. Chem. B 107 (2003) 66.
[78] S. Nishihara, T. Akutagawa, T. Hasegawa, T. Nakamura, Inorg. Chem. 42 (2003) 2480.
[79] T. Akutagawa, K. Shitagami, S. Nishihara, S. Takeda, T. Hasegawa, T. Nakamura, Y. Hosokoshi, K. Inoue, S. Ikeuchi, Y. Miyazaki, K. Saito, J. Am. Chem. Soc. 127 (2005) 4397.
[80] S. Ikeuchi, Y. Miyazaki, S. Takeda, T. Akutagawa, S. Nishihara, T. Nakamura, K. Saito, J. Chem. Phys. 123 (2005) 044514.
[81] S. Nishihara, T. Akutagawa, T. Hasegawa, T. Nakamura, Chem. Commun. 2002 (2002) 408.
[82] S. Nishihara, T. Akutagawa, T. Hasegawa, S. Fujiyama, T. Nakamura, T. Nakamura, J. Solid State Chem. 168 (2002) 661.
[83] I.V. Kozhevnikov, Chem. Rev. 98 (1998) 171.
[84] Handbook of Chemistry and Physics, 83rd ed., CRC Press, New York, 2002.
[85] T. Akutagawa, D. Endo, H. Imai, S. Noro, L. Cronin, T. Nakamura, Inorg. Chem. 45 (2006) 8626.
[86] P.J. Nirgey, Cryst. Growth 40 (1977) 265.
[87] M. Sadakane, E. Steckhan, Chem. Rev. 98 (1998) 219.
[88] S. Himeno, M. Takamoto, R. Santo, A. Ichimura, Bull. Chem. Soc. Jpn. 78 (2005) 95.
[89] T. Akutagawa, G. Saito, Bull. Chem. Soc. Jpn. 68 (1995) 1753.
[90] T. Akutagawa, G. Saito, M. Kusunoki, K. Sakaguchi, Bull. Chem. Soc. Jpn. 69 (1996) 2487.

[91] T. Akutagawa, T. Hasegawa, T. Nakamura, T. Inabe, G. Saito, Chem. Eur. J. 8 (2002) 4402.
[92] M.T. Pope, Heteropoly and Isopoly Oxometalates, Springer-Verlag, Berlin, 1983, p. 109.
[93] M.B. Robin, P. Day, Adv. Inorg. Chem. Radiochem. 10 (1967) 248.
[94] B. Movaghar, L. Schweitzer, H. Overhof, Phil. Mag. B 37 (1978) 683.
[95] R. Bachus, B. Movaghar, L. Schweitzer, U. Voget-Grote, Phil. Mag. B 39 (1979) 27.
[96] I.G. Austin, N.F. Mott, Adv. Phys. 18 (1969) 41.
[97] N.F. Mott, Metal–Insulator Transition, 2nd ed., Taylor & Francis, 1990.
[98] G.A. Jeffrey, in: D.G. Truhlar (Ed.), An Introduction to Hydrogen Bonding, Oxford University Press, New York, 1997.
[99] T. Steiner, Angew. Chem. Int. Ed. Engl. 41 (2002) 48.
[100] A. Bondi, J. Phys. Chem. 68 (1964) 441.
[101] R.L. Carlin, Magnetochemistry, Springer-Verlag, Heidelberg, 1986.
[102] J.P. Poblet, X. López, C. Bo, Chem. Soc. Rev. 32 (2003) 297.
[103] X. López, J.M. Maestre, C. Bo, J.-M. Poblet, J. Am. Chem. Soc. 123 (2001) 9571.
[104] Y. Li, N. Hao, E. Wang, M. Yuan, C. Hu, N. Hu, H. Jia, Inorg. Chem. 42 (2003) 2729.
[105] V. Hivaiah, S.K. Das Samar, Inorg. Chem. 44 (2005) 7313.
[106] W. Yang, C. Lu, X. Lin, H. Zhuang, Chem. Commun. 2000 (2000) 1623.
[107] Y. Jeannin, J. Cluster Sci. 3 (1992) 55.
[108] M.H. Alizadeh, S.P. Harmalker, Y. Jeannin, J. Martin-Frere, M.T. Pope, J. Am. Chem. Soc. 107 (1985) 2662.
[109] J. Creaser, M.C. Heck, R.J. Neitz, M.T. Pope, Inorg. Chem. 32 (1993) 1573.
[110] M.R. Antonio, L. Soderholm, Inorg. Chem. 33 (1994) 5988.
[111] L. Soderholm, G.K. Liu, J. Muntean, M.R. Antonio, J. Phys. Chem. 99 (1995) 9611.
[112] D.-L. Long, H. Abbas, P. Kögerler, L. Cronin, J. Am. Chem. Soc. 126 (2004) 13880.
[113] D.-L. Long, O. Brucher, C. Streb, L. Cronin, Dalton Trans. 2006 (2006) 2852.
[114] A. Müller, E. Krickemeyer, H. Bögge, M. Schmidtmann, B. Botar, M.O. Talismanova, Angew. Chem. Int. Ed. Engl. 42 (2003) 2085.
[115] D.L. Long, P. Kögerler, L. Cronin, Angew. Chem. Int. Ed. Engl. 43 (2004) 1817.
[116] D.L. Long, H. Abbas, P. Kögerler, L. Cronin, Angew. Chem. Int. Ed. Engl. 44 (2005) 3415.
[117] A. Tsuda, E. Hirahara, Y.-S. Kim, H. Tanaka, T. Kawai, T. Aida, Angew. Chem. Int. Ed. Engl. 43 (2004) 6327.
[118] A. Müller, E. Krickemeyer, H. Bögge, M. Schmidtmann, S. Roy, A. Berkle, Angew. Chem. Int. Ed. Engl. 41 (2002) 3604.
[119] A. Müller, B. Botar, H. Bögge, P. Kögerler, A. Berkle, Chem. Commun. 2002 (2002) 2944.
[120] A. Müller, S.K. Das, S. Talismanov, S. Roy, E. Beckmann, H. Bögge, M. Schmidtmann, A. Merca, A. Berkle, L. Allouche, Y.S. Zhou, L.J. Zhang, Angew. Chem. Int. Ed. Engl. 42 (2003) 5039.
[121] A. Müller, D. Rehder, E.T.K. Haupt, A. Merca, H. Bögge, M. Schmidtmann, G. Heinze-Brückner, Angew. Chem. Int. Ed. Engl. 43 (2004) 4466.
[122] E.T.K. Haupt, C. Wontorra, D. Rehder, A. Müller, Chem. Commun. 44 (2005) 3912.
[123] A. Müller, L. Toma, H. Bögge, C. Schäffer, A. Stammler, Angew. Chem. Int. Ed. Engl. 44 (2005) 7757.
[124] A. Müller, Y. Zhou, H. Bögge, M. Schmidtmann, T. Mitra, E.T.K. Haupt, A. Berkle, Angew. Chem. Int. Ed. Engl. 45 (2006) 460.